Aftershock Observation and Analysis of the 2013 M_s 7.0 Lushan Earthquake

by Lihua Fang, Jianping Wu, Weilai Wang, Wenkang Du, Jinrong Su, Changzai Wang, Ting Yang, and Yan Cai

Online Material: Figures of station deployment time and of spatial and temporal depiction of aftershocks, and tables of station information and aftershock catalogs.

INTRODUCTION

At 08:02 (local and Beijing time) on 20 April 2013, an earthquake of M_s 7.0 (M_w 6.6) struck Lushan County in Sichuan Province, southwestern China (hereafter referred to as the Lushan earthquake). The Lushan earthquake resulted in casualties and severe damage to the buildings and to the economic activities of the region. The earthquake left 193 dead, up to 10,000 injured, and 25 missing. The direct economic loss hit over $1.6 billion U.S.

The Lushan earthquake is the second destructive earthquake to have occurred in the southern segment of the Longmenshan fault zone since the 12 May 2008 M_s 8.0 Wenchuan earthquake (Fig. 1). The distance between the epicenters of the Lushan earthquake and the Wenchuan earthquake is about 87 km (Fang, Wu, Wang, Lü, *et al.*, 2013). As happened following the Wenchuan earthquake, the occurrence of the Lushan earthquake also stimulated lots of discussions on the seismic risk potential and prediction in southwest China. In particular, whether it was a large aftershock of the Wenchuan earthquake has been heatedly debated (Chen *et al.*, 2013; Du *et al.*, 2013; J. Liu *et al.*, 2013; Wang *et al.*, 2013; Jia *et al.*, 2014).

The Longmenshan fault zone is a tectonic boundary that separates the eastern Tibetan plateau to the west and the rigid Sichuan basin to the east. The major faults in the southern segment of the Longmenshan fault zone include the Yanjing–Wulong fault, Dachuan–Shuangshi fault, Xinkaidian fault, and Dayi fault. Because the Lushan earthquake did not produce obvious surface ruptures, the causative fault of this event is also a subject of debate (Chen *et al.*, 2014; Xu *et al.*, 2013; Y. Zhang *et al.*, 2013).

Some researchers conducted earthquake relocation, shear-wave splitting, and earthquake tomography after the Lushan earthquake (Fang, Wu, Wang, Lü, *et al.*, 2013; Jiang *et al.*, 2013; Li *et al.*, 2013; Zhang and Lei, 2013; Zeng *et al.*, 2013; Lei *et al.*, 2014; Pei *et al.*, 2014; Long *et al.*, 2015). These results, together with the focal mechanism (Lü *et al.*, 2013; Zeng *et al.*, 2013; Han *et al.*, 2014) and rupture process of the mainshock (C. L. Liu *et al.*, 2013; Wang *et al.*, 2013; Y. Zhang *et al.*, 2013; C. P. Zhao *et al.*, 2013), and the relation with the stress change caused by the mainshock (Miao and Zhu, 2013), provide evidence for the understanding of the source process of the mainshock and the generation of the aftershocks. These results also provide heuristic clues to the seismic hazard of the seismic gap between the Lushan earthquake sequence and the Wenchuan earthquake sequence (Gao *et al.*, 2013). However, most of these studies used only several days' aftershock observation data and limited our understanding of the Lushan earthquake.

After the Lushan event, we deployed 35 temporary seismic stations in the vicinity of the epicentral region. The temporary stations, combined with the permanent stations, covered the epicentral area very well, allowing us to determine the aftershock locations with high precision and to delineate the geometry of the seismogenic fault clearly. This study describes the aftershock observation and analysis following the Lushan earthquake, which included rapid deployment of temporary stations in the field for real-time seismic monitoring purposes and scientific investigation, aftershock analysis and relocation, and delineation of the geometry of seismogenic fault. These results are helpful for understanding seismogenic structure of the earthquake and provide a lot of useful basic information for further specific studies and hazard assessment.

AFTERSHOCK OBSERVATION

Temporary seismic networks are an important element in the response to earthquake emergency. They improved the detection performance of permanent monitoring systems during seismic sequences. The improvement in earthquake detection and location capabilities can be important for decision makers to assess the current situation and can provide invaluable data for scientific studies related to hazard, tectonics, and earthquake physics. Temporary seismic networks usually have been deployed for $M_L \geq 5.0$ crustal earthquakes that have occurred in the Chinese mainland (e.g., Fang *et al.*, 2011; Fang, Wu, Wang, Wang, and Yang, 2013). They have been important

doi: 10.1785/0220140186

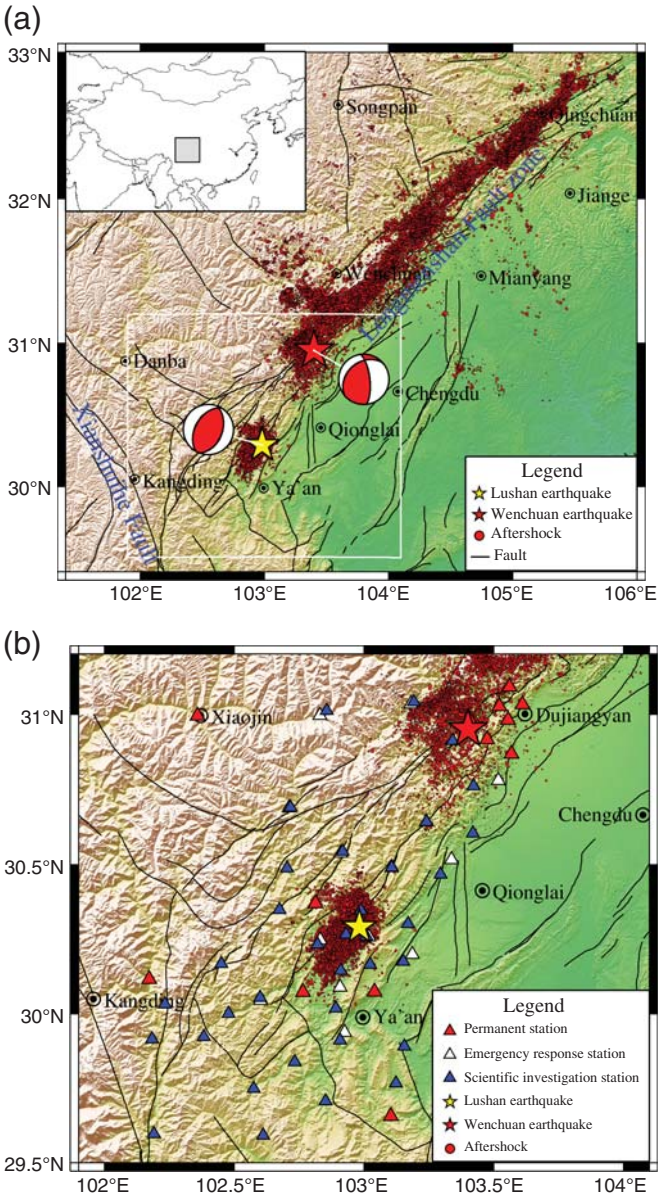

▲ **Figure 1.** (a) Tectonic settings of the Longmenshan fault zone. Red and yellow stars indicate the epicenters of the Wenchuan and Lushan earthquakes, respectively. The focal mechanisms of the Lushan earthquake and Wenchuan earthquake are also shown. Red circles represent aftershocks of the Lushan and Wenchuan earthquakes. Black lines indicate the main faults. The inset map shows the location of the study region in the Chinese mainland. (b) The distribution of seismic stations in and around the epicentral region of the Lushan earthquake. Permanent seismic stations are shown as red triangles. Temporary seismic stations, deployed in the emergence response phase and the scientific investigation phase, are shown as white and blue triangles, respectively.

monitoring and scientific tools to better understand the seismic sequences (Fang, Wu, Wang, Lü, *et al.*, 2013; McNamara *et al.*, 2013; Govoni *et al.*, 2014).

Within the first few days of the M_s 7.0 Lushan earthquake, multiple government and academic institutions deployed seismic instruments near the epicenter. The primary objective of temporary deployment of the seismic stations is to record and document the distribution of aftershocks to delineate the causative fault and constrain the dimensions of the rupture zone. The first real-time station started operating at about 19:25 p.m. on 20 April 2013. A total of 15 temporary seismograph stations were deployed within five days of the mainshock (Fig. 1 and Ⓔ Fig. S1, available in the electronic supplement to this article). Most of the stations were set up in the apartments of local residents. All stations recorded data continuously onsite with a sampling rate of 100 Hz. Most of the stations are powered with solar panels. The waveform data were telemetered to the Sichuan Seismological Network Center and transferred to the Data Manage Center of the China Seismic Array at the Institute of Geophysics, China Earthquake Administration (IGPCEA). This ensured substantial improvements in the real-time monitoring of the aftershock sequence.

One month after the Lushan earthquake, the China Earthquake Administration carried out the scientific investigation of the 2013 Lushan earthquake. In an effort to monitor the seismic activity of the seismic gap between the Lushan earthquake sequence and the Wenchuan earthquake sequence and to enhance the observations of the Lushan aftershock sequences, IGPCEA deployed 20 more temporary stations around the epicentral area, increasing the number of temporary stations to 35 and making it the best-recorded aftershock sequence in the Chinese mainland.

Each seismic station was equipped with a 24-bit recorder (REF TEK/EDAS-24IP) with a Global Positioning System timing system. Among them, 13 stations were installed with short-period seismometers (CMG-40T), and 22 stations were equipped with broadband sensors (CMG-3ESPC and CMG-3T). The 15 temporary stations deployed in the emergency rapid-response phase were moved to new locations to reduce the ambient noise. Most of the seismometers were deployed in pits with 1.5 m depth, which substantially reduced the noise level and enhanced the monitoring capability. The seismic stations cover the aftershock region with an average azimuthal gap less than 150°. The distances between stations and epicenters vary from 0.1 to 200 km. Both the permanent stations, combined with the portable stations temporarily deployed within the epicentral region, enabled detection and location of a complete earthquake catalog down to approximately M_L 0.8. Ⓔ Table S1 and Figure S1 list the detailed station information, including the station coordinates, and starting and ending times.

DATA PROCESSING

The Lushan earthquake was followed by a productive aftershock sequence. By the end of 24:00:00 (local time) on 20 April 2014, 14,482 aftershocks were recorded by the temporary seismic network. The magnitude of the aftershocks ranges from $M_L - 0.5$ to 5.6. There are 6 aftershocks with $M_L \geq 5.0$ and 54 aftershocks with $M_L \geq 4.0$. Figure 2a shows the magnitude–time diagram of the aftershock sequence. Figure 2b shows the number of aftershocks per day from 20 April 2013 to 20 April 2014.

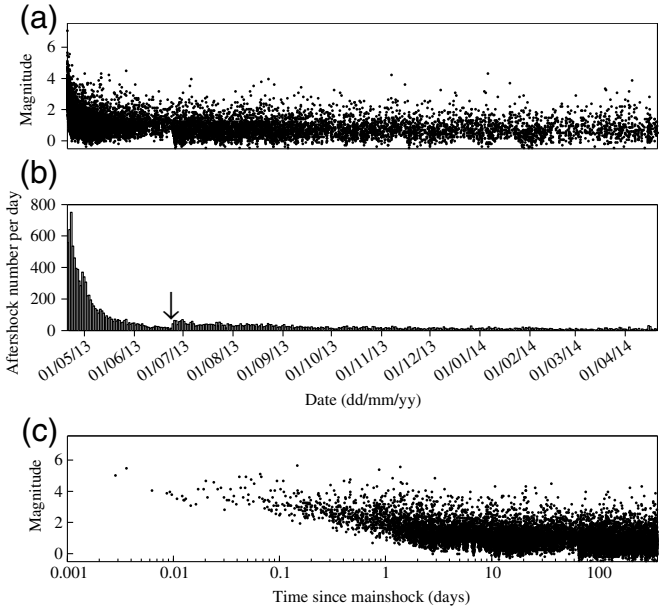

▲ **Figure 2.** (a) The magnitude–time plot of the aftershock sequence from 20 April 2013 to 20 April 2014. (b) Number of recorded aftershocks per day. The down arrow indicates the significant enhancement of the monitoring capability due to the operation of the temporary seismic stations deployed in the scientific investigation phase. (c) Magnitude compared with logarithmic time since the mainshock.

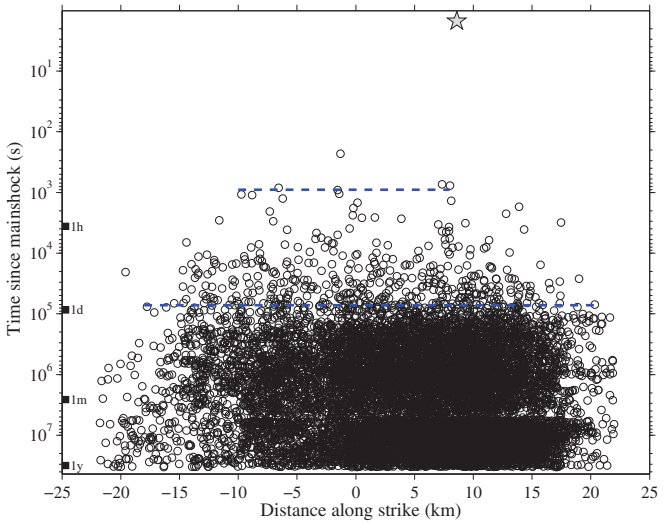

▲ **Figure 3.** The occurrence time of aftershocks since the Lushan mainshock as a function of distance along the strike. The black circles represent the aftershocks. The gray star is the mainshock. The upper and lower blue dashed lines, respectively, mark the 15 min and 20 hr time intervals after the mainshock.

During the first week of the sequence, the rate of seismicity remained high, with more than 300 events per day. The aftershock sequence of the Lushan earthquake decays gradually on the whole. The earthquake activity shows an increase two months after the mainshock, which is due to the enhancement of the monitoring capability by increasing the temporary seismic stations. Figure 2c is similar to Figure 2a but with logarithmic time.

P- and *S*-wave arrivals were picked by visual inspection by analysts at the Sichuan Seismological Network Center. *P* and *S* waves were picked on the vertical and horizontal components, respectively. There are 111,474 *P* arrivals and 110,532 *S* arrivals picked for the 14,482 events. On average, each event has 15 phase readings.

Initial event locations were obtained using program LOC3D based on a 3D velocity model (Wu *et al.*, 2009; Fang, Wu, Wang, Lü, *et al.*, 2013). This earthquake location program has been well tested and applied extensively in the Sichuan and Yunnan region. The 3D velocity model was constructed using the body-wave tomography method (Zhao *et al.*, 1992, 1994). The location program calculates theoretical arrival times of regional phases using the pseudobending technique. The program also takes topography and station elevation into consideration in the ray tracing. The average root mean square (rms) of the travel-time residual in the initial catalog is 0.17 s. The average location error of the hypocenters is 0.85 and 2.7 km in the horizontal and vertical components, respectively. Ⓔ Table S2 is the initial catalog.

Although the catalog is not complete immediately after the mainshock, it still provides much useful information for the evolution of the aftershock activity. Figure 3 shows the expansion of the aftershock zone. The area of the aftershocks expands from ~18 km at 15 min to ~39 km at 20 hr after the mainshock. Figure 3 also reveals that most of the aftershocks clustered around the mainshock. We compute the *b*-value and magnitude of completeness (M_c) using ZMAP (Wiemer, 2001). Figure 4a shows the cumulative number of earthquakes observed as a function of magnitude, which is used to determine a *b*-value for the aftershock sequence. Using a maximum-likelihood algorithm (Wiemer, 2001) results in a catalog of aftershocks that is complete to M_L 1.0 and has a *b*-value of 0.7 ± 0.01. The *b*-value shows slight variation over time (Fang *et al.*, 2014). Plotting M_c with time reveals a decreased magnitude threshold due to the operation of the temporary seismic network. This *b*-value is consistent with a previous broad area study before the Lushan earthquake in the Longmenshan fault zone (Yi *et al.*, 2013). The low *b*-value indicates the high stress state in the southern segment of Longmenshan fault zone.

The magnitude of completeness M_c reflects the detection threshold of a seismic network. The lower the M_c, the higher the monitoring capability. As displayed in Figure 4b, the M_c changed through time with three distinct phases. The first two days of the sequence had the highest M_c but then dropped off quickly into the second phase. After 24 June 2013, the M_c declined again, where it remained relatively constant afterward. The mean interstation distance in the Lushan seismic array is about 14 km, which is larger than that deployed in the 2011 Mineral, Virginia, earthquake and the 2012 Emilia earthquake source regions (McNamara *et al.*, 2013; Govoni *et al.*, 2014). However, the magnitude of completeness M_c is lower than for

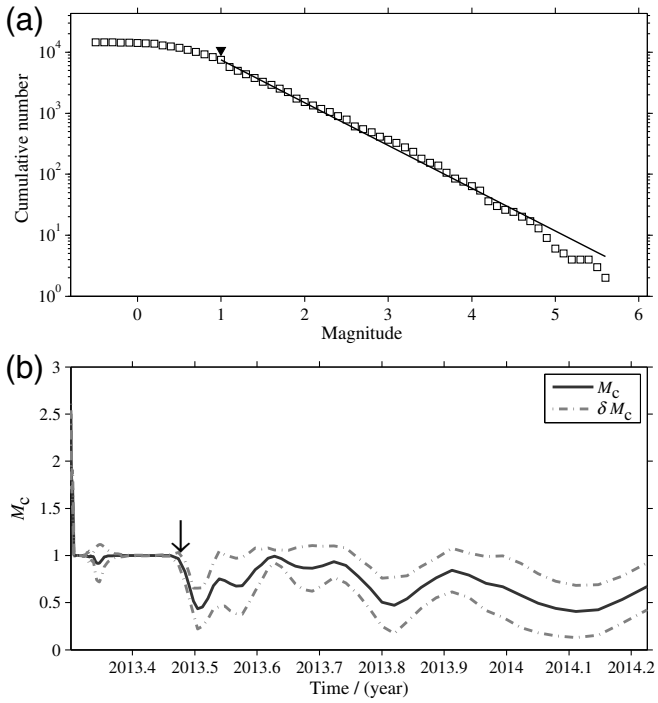

▲ **Figure 4.** (a) The frequency–magnitude distribution map of the source region. The inverted triangle indicates the magnitude of completeness M_c. The cumulative numbers of earthquakes are shown by squares. The line represents the maximum-likelihood fit to the data. (b) Plot of M_c versus time since the mainshock and the uncertainty $M_c \pm \delta M_c$. The down arrow marks the operating time of the 35 temporary seismic stations.

the Mineral and Emilia earthquakes. This reflects the low-ambient noise level of the Lushan seismic array.

RELOCATION OF AFTERSHOCKS USING HYPODD

To better constrain the spatial pattern of aftershocks, we applied the double-difference algorithm *hypoDD* to refine the relative hypocentral locations (Waldhauser and Ellsworth, 2000). This program minimizes errors introduced to earthquake locations by unmodeled 2D or 3D velocity structure by assuming that the spatial separation between hypocenters is small compared to the hypocenter–station distance, and therefore velocity variation is the same along event-pair ray paths.

We did not relocate all observed aftershocks, but only those events for which there were a sufficient number of arrival-time observations and good azimuthal coverage to ensure the well-delineated fault geometry. The event selection criteria are initial horizontal location error less than 1.0 km and vertical location error less than 2.0 km, rms < 0.4 s, largest azimuthal gap less than 120°, at least eight *P*- and two *S*-wave readings, at least four stations within 30 km epicentral distance, and minimum epicentral distance less than 10 km. Events meeting the data selection criteria were input into the *hypoDD* relocation program. Only the phase arrival time picked by the analysts is used in relocation. We obtained a representative subset of 1993 aftershocks for the subsequent inversion.

Table 1
1D Velocity Model Used in *hypoDD* Relocation

P-Wave Velocity (km/s)	Depth (km)
5.30	0
6.05	4
6.35	17
6.75	28
7.00	39
8.15	45

The 1D *P*-wave velocity model is taken from a seismic refraction profile located about 15 km south of the source region (Table 1; Wang *et al.*, 2007). The ratio of V_P to V_S is set to 1.73. Eight iterations were used for the conjugate gradient method (least-squares [LSQR]) when relocating with *hypoDD*. The travel-time differences were calculated for the event pairs separated by less than 5 km. The maximum distance between cluster centroid and station was 150 km. Only events with a maximum of eight neighbors linked to each other were considered for the relocation. The *a priori* weights of *P* and *S* waves were 1.0 and 0.5, respectively. The condition numbers (i.e., ratio of the largest to smallest eigenvalues) obtained for the eight iterations range from 65 to 80. A total of 1993 earthquakes were obtained with *hypoDD*. The final double-difference locations have average rms residuals of 0.07 s. Relative location uncertainties have medians of 65 m laterally and 73.5 m vertically. Relocation errors given by LSQR against the singular value decomposition result were checked to ensure the consistency in hypocenters. Compared with the initial results, the location errors were significantly reduced by the double-difference location algorithm. Ⓔ Table S3 is the aftershock catalog relocated using *hypoDD*.

Figure 5 shows the map view of the epicenters, and Figure 6 shows the cross-section view of the hypocenters. The vertical cross section A–A′ is drawn roughly parallel to the strike of the mainshock rupture planes (N48°E); the vertical cross sections going from B–B′ to E–E′ are drawn roughly perpendicular to this strike. We project the earthquakes located within 3.0 km distance from the vertical plane on the cross sections going from B–B′ to E–E′, whereas on the cross section A–A′ the whole set of analyzed earthquakes is projected.

The epicenter of the Lushan earthquake was located to the east side of the Dachuan–Shuangshi fault and to the northeast part of the source region. The distribution of relocated epicenters defines a northeast-trending aftershock zone covering an area of 55 km × 25 km. Most of the aftershocks are distributed near the surface trace of the Dachuan–Shuangshi fault. Some earthquakes were in the southern part of aftershock region, but more were in the mid-northern section. The width of the aftershock area changes near Lushan, being wide in the area north of Lushan and narrow in the south.

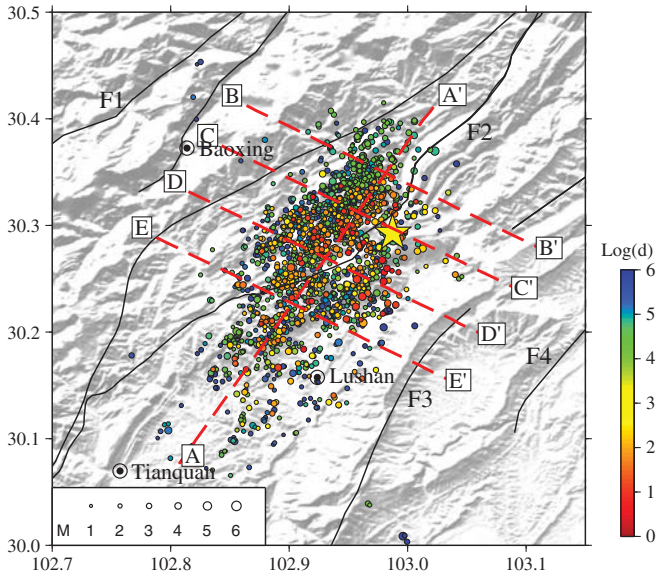

▲ **Figure 5.** Map view of the aftershock epicenters relocated with *hypoDD*. Earthquakes are sized by magnitude and color-coded by the logarithmic time after the mainshock (yellow star). The red dotted lines show the locations of the cross sections. Black lines represent the main faults: F1, Yanjing–Wulong fault; F2, Dachuan–Shuangshi fault; F3, Xinkaidian fault; and F4, Dayi fault. The background of the map is the topography.

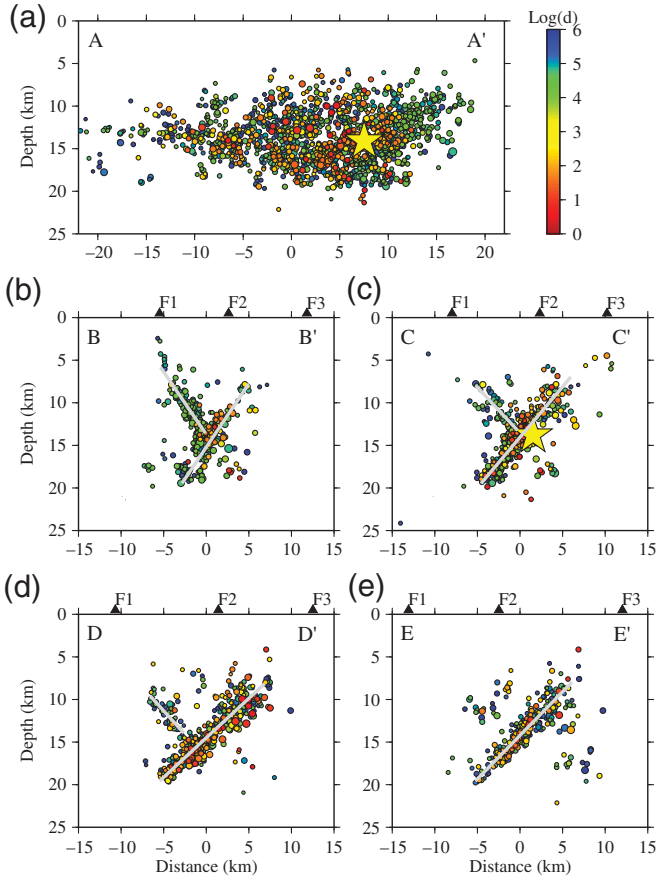

▲ **Figure 6.** Cross sections of the hypocenters of the aftershocks relocated with *hypoDD*. The yellow star indicates the mainshock of the Lushan earthquake. On each cross section, the fault traces are shown as triangles. Other symbols are the same as in Figure 5. The gray lines show the fault planes fitted with the linear regression method. On the along-strike cross section A–A′, we project all the events on the vertical plane. On the cross sections going from B–B′ to E–E′, we project the earthquakes located within 3 km from the vertical planes.

The cross sections in Figure 6 show that most of the hypocenters are confined between 5 and 20 km depth. There are a small number of aftershocks in the shallow crust. Along cross section A–A′, the focal depth changes significantly. The focal depths are confined between 10 and 20 km in the southwest part of the profile, whereas there are some shallow aftershocks in the northeast part. There is a southeast-dipping fault intersecting with the northwest-dipping fault in a *y* shape. Our high-precision relocation results image the *y*-shaped fault more obviously than the previous studies. The *y*-shaped fault system is clearly recognized in the northeast part of the source region but blurred in the southwest part. The mainshock was located at the intersection of the two faults. The relocated aftershocks indicate that at least two intersecting faults, or a fault system, were activated during the Lushan earthquake sequence. The southeast-dipping fault may be a back thrust fault that was activated about 3 hr after the mainshock (Ⓔ Fig. S3).

DISCUSSION

Our new relocation results represent a sensible improvement on the existing one in terms of geometrical definition of the seismogenic fault system, whose characteristics are here more clearly recognizable. Several groups relocated the aftershock sequences of the Lushan earthquake (e.g., Lü *et al.*, 2013; Su *et al.*, 2013; Zhang and Lei, 2013). Their results provide preliminary constraints on the seismotectonic interpretation of the Lushan earthquake. However, the fine-scale fault geometry was not well imaged in the previous studies. For example, the *y*-shaped fault system and sharp fault planes have been shown vaguely in Han *et al.* (2014) and Long *et al.* (2015) and are not revealed in Lü *et al.* (2013) and Zhang and Lei (2013). This may be due to the different datasets and earthquake location methods they used, because most of them used only several days' aftershock data recorded by the permanent seismic stations.

In our previous study, we relocated the aftershocks of the Lushan earthquake using one-week data after the mainshock (Fang, Wu, Wang, Lü, *et al.*, 2013). The aftershock distribution obtained using the two dataset are very similar. Both results reveal the *y*-shaped fault system in the source area. This indicates that the late aftershock activity does not change greatly with time. However, the new relocation results reveal a sharper fault plane than described in previous studies owing to the operation of more temporary seismic stations.

The focal mechanism solution of the mainshock suggests that the Lushan earthquake is associated with a thrust fault

(Zeng *et al.*, 2013; Han *et al.*, 2014). The strikes determined by fault-plane solutions are mostly oriented northeast and show a good consistency with the trend of the aftershock distribution. However, the dip of the fault plane determined using different datasets and methods varies from 33° to 47° (Lü *et al.*, 2013; Zeng *et al.*, 2013; B. Zhao *et al.*, 2013; Han *et al.*, 2014). The differences in the fault dip may be caused by the different frequency waves they used and also indicate the complexity of the seismogenic fault. From the cross sections in Figure 6, we estimate the dip of the faults with the linear regression method. The dip angles for the four profiles from northeast to southwest are 56°, 50°, 43°, and 46°, respectively. The dip angle becomes more gentle from the northeast to the southwest, although there is a slight increase in the southwest end. It is not surprising there is a difference in the fault dip determined using least-squares fitting of aftershocks and focal mechanisms. The dip given by focal mechanisms shows a mean dip of the fault, whereas the dip determined with aftershock distribution reflects the lateral variation of fault geometry. Compared to some continental thrust earthquakes, such as the 1994 Northridge earthquake (35°; Hauksson *et al.*, 1995) and the 1999 Chi-Chi earthquake (34°; Chang *et al.*, 2000), the Lushan earthquake occurred on a relatively high-dip-angle thrust fault. Moreover, the magnitude of the Lushan earthquake is relatively small (M_w 6.6). Thus, it was difficult for the mainshock to breach the surface. It is worth noting that most of the aftershocks are located to the southwest of the mainshock (Figs. 5 and 6). The rupture model also indicates that the slip propagates to the southwest (Hao *et al.*, 2013). Pei *et al.* (2014) believes that the seismicity gap between the Wenchuan and Lushan earthquakes is weak and the upper crust is likely ductile. Thus might act as a barrier for ruptures for the two earthquakes. Both the high dip angle of the fault in the northeastern part and the ductile upper crust in the seismicity gap make it difficult to rupture to the northeast.

Earthquake rupture studies show that the slip distribution is dominated between 5 and 20 km depth range and the rupture does not reach the surface (Hao *et al.*, 2013; Y. Q. Zhang *et al.*, 2014). Geologic investigations following the Lushan earthquake found no coseismic surface rupture (Xu *et al.*, 2013; Chen *et al.*, 2014). Therefore, it is difficult to associate the causative fault with any previously mapped faults. The seismogenic fault of the Lushan earthquake remains controversial. The southern part of the Longmenshan fault system is composed of a series of imbricated reverse faults dipping to the northwest. From southeast to northwest, these are the Dayi, Xinkaidian, Dachuan–Shuangshi, and Yanjing–Wulong faults (Fig. 5). Xu *et al.* (2013) speculate that the Lushan earthquake occurred on a propagating blind thrust fault underneath a growing fold on the basis of relative positions between aftershock distribution and anticline. Zhang and Lei (2013) infer that the Lushan earthquake probably occurred at the intersection of the detachment surface at the base of the Longmenshan fault zone and the Shangshi–Dachuan fault. Xu and Xu (2014) analyzed the landslide data in and around the Lushan source area. They found that the landslide density changes suddenly about 1–2 km from the western Shangli fault (Xinkaidian fault) to the northwest, and the landslide density on the footwall of the fault is clearly lower than that of the hanging wall. Xu and Xu (2014) concludes that the seismogenic fault for the Lushan earthquake is probably the western Shangli fault (Xinkaidian fault). The distribution of the aftershocks indicates that the seismogenic structure is a *y*-shaped fault system located to the east of the Dachuan–Shuangshi fault (Fig. 6). We interpret the southeast-dipping fault as a back-thrust fault. Seismic reflection profiles reveal that the back-thrust faults exist in the south segment of Longmenshan fault (Li *et al.*, 2014). The two intersecting faults were activated during the Lushan earthquake. Most aftershocks are confined between 5 and 20 km depth. Extrapolation of the main thrust fault to the surface roughly aligns with the surface trace of the Xinkaidian fault. The high-resolution aftershock relocation results lend support to the inference that the Lushan earthquake occurred on a blind thrust fault located to the east of Dachuan–Shuangshi fault.

The source region of the Lushan earthquake is characterized by a low *b*-value of 0.7 ± 0.01. This *b*-value is consistent with a previous study in the south segment of Longmenshan fault zone (Yi *et al.*, 2013). Wyss (1973) argues that there is a negative correlation between the observed *b*-value and the level of stress accumulated in and around the source volume. Regions with low *b*-value may be interpreted as possible asperities (stress concentrations) reflecting variations in frictional properties along the fault, which may control the recurrence of the next large event (McNamara *et al.*, 2013). Similar to the 1944 Northridge earthquake sequence (Hauksson *et al.*, 1995), the focal mechanisms of large aftershocks of the Lushan earthquake show relative uniformity of thrust type (Lü *et al.*, 2013; B. Zhao *et al.*, 2013). This indicates that the stress release in the mainshock was not complete. The hazard assessment based on the change in the Coulomb failure stress and balancing seismic moments in the Longmenshan fault zone indicate that the Lushan earthquake released only about 1/3 of the estimated moment deficit on the southern Longmenshan fault (Liu *et al.*, 2014). These results suggest that the potential seismic hazard in the southern segment of Longmenshan fault zone remains high.

CONCLUSIONS

We provided a detailed description of the aftershock observation and analysis of the 2013 M_s 7.0 Lushan earthquake based on a combined dataset, including both permanent and temporary seismic stations. Our new relocation results provide a sensible improvement on the existing ones in terms of earthquake location accuracy and geometrical definition of the seismogenic fault system.

The precisely relocated aftershocks define a rupture that extends between approximately 5–20 km in depth and 55 km along the strike of the fault plane. The aftershocks delineate the geometry of the main thrust fault that strikes N48°E and dips to the northwest around 50°. Extrapolation of the fault plane of the main thrust fault to the surface roughly aligns with

the surface trace of the Xinkaidian fault. A back thrust fault was imaged in the source region that was seldom found elsewhere via earthquake relocation. The *y*-shaped fault system should be considered when studying kinematic rupture models of the Lushan earthquake. The aftershock relocation results, in conjunction with geologic investigations, focal mechanism solutions, and source rupture models, support the hypothesis that the seismogenic structure of the Lushan earthquake is a blind thrust fault located to the east of the Dachuan–Shuangshi fault.

We presented a complete aftershock sequence catalog of the Lushan earthquake for the period from 20 April 2013 to 20 April 2014. The catalog is of great importance for comparison with automatic processing procedures and detection of missing early aftershocks (Peng and Zhao, 2009). This study also paves the way for future investigations of the Lushan earthquake, such as statistical seismology (Jia *et al.*, 2014), tomographic inversion of deep velocity structure (Li *et al.*, 2013; Lei *et al.*, 2014), and hazard assessment.

ACKNOWLEDGMENTS

The aftershock observation and analysis of the Lushan earthquake required a large number of dedicated people. The authors greatly appreciate the rapid response and hard work of the field crews. The crews included Jiansi Yang, Xudong Jiang, Zhiqiang Xu, Yu Zheng, Liang Shen, Peng Wu, and additional staff from the Institute of Geophysics, China Earthquake Administration. Zhongliang Wu provided valuable comments on early versions of the manuscript. This work was supported by China National Special Fund for Earthquake Scientific Research in Public Interest (Grant Number 201408014), National Science Foundation Grant of China (Grant Number 41304043), and Scientific Investigation of April 20, 2013 **M** 7.0 Lushan, Sichuan, Earthquake sponsored by China Earthquake Administration.

REFERENCES

Chang, C. H., Y. M. Wu, T. C. Shin, and C. Y. Wang (2000). Relocation of the 1999 Chi-Chi earthquake in Taiwan, *Terr. Atmos. Ocean. Sci.* **11,** no. 3, 581–590.

Chen, L. C., H. Wang, Y. K. Ran, S. X. Lei, X. Li, F. Y. Wu, X. Q. Ma, C. L. Liu, and F. Han (2014). The 2013 Lushan M_s 7.0 earthquake: Varied seismogenic structure from the 2008 Wenchuan earthquake, *Seismol. Res. Lett.* **85,** no. 1, 34–39, doi: 10.1785/0220130109.

Chen, Y. T., Z. X. Yang, Y. Zhang, and C. Liu (2013). A brief talk on the 20 April 2013 Lushan M_w 6.7 earthquake, *Acta Seismol. Sinica* **35,** 285–295, doi: 10.3969/j.issn.0253-3782.2013.03.001 (in Chinese with English abstract).

Du, F., F. Long, X. Ruan, G. X. Yi, Y. Gong, M. Zhao, Z. W. Zhang, H. Z. Qiao, Z. Wang, and J. Wu (2013). The M 7.0 earthquake and the relationship with the M 8.0 Wenchuan earthquake in Sichuan, China, *Chin. J. Geophys.* **56,** 1772–1783, doi: 10.6038/cjg20130535 (in Chinese with English abstract).

Fang, L. H., C. S. Jiang, S. F. Zhang, and H. Jiang (2014). Aftershock sequence: Monitoring and analysis, in *Earthquake Phenomenology from the Field: The April 20, 2013, Lushan Earthquake*, Z. L. Wu, C. S. Jiang, X. J. Li, G. J. Li, and Z. F. Ding (Editors), Springer Briefs in Earth Sciences, Springer-Verlag, Singapore, 33–45, doi: 10.1007/978-981-4585-15-6_4.

Fang, L. H., J. P. Wu, W. L. Wang, Z. Y. Lü, C. Z. Wang, T. Yang, and Y. Cai (2013). Relocation of mainshock and aftershock sequences of M_s 7.0 Sichuan Lushan earthquake, *Chin. Sci. Bull.* **58,** 3451–3459, doi: 10.1007/s11434-013-6000-2.

Fang, L., J. Wu, C. Wang, W. Wang, and T. Yang (2013). Relocation of the 2012 M_s 6.6 Xinjiang Xinyuan earthquake sequence, *Sci. China Earth Sci.* **57,** no. 2, 216–220, doi: 10.1007/s11430-013-4755-6.

Fang, L. H., J. P. Wu, T. Z. Zhang, J. Huang, C. Z. Wang, and T. Yang (2011). Yunnan Yingjiang M_s 5.8 earthquake and its aftershock sequence relocations, *Acta Seismol. Sinica* **33,** 262–267 (in Chinese with English abstract).

Gao, Y., Q. Wang, B. Zhao, and Y. T. Shi (2013). A rupture blank zone in middle south part of Longmenshan faults: Effect after Lushan M_s 7.0 earthquake of 20 April 2013 in Sichuan, China, *Sci. China Earth Sci.* **43,** 1038–1046, doi: 10.1007/s11430-013-4646-x (in Chinese).

Govoni, A., A. Marchetti, P. De Gori, M. Di Bona, F. P. Lucente, L. Improta, C. Chiarabba, A. Nardi, L. Margheriti, N. P. Agostinetti, *et al.* (2014). The 2012 Emilia seismic sequence (northern Italy): Imaging the thrust fault system by accurate aftershock location, *Tectonophysics* **622,** 44–55, doi: 10.1016/j.tecto.2014.02.013.

Han, L., X. Zeng, C. Jiang, S. Ni, H. Zhang, and F. Long (2014). Focal mechanisms of the 2013 M_w 6.6 Lushan, China earthquake and high-resolution aftershock relocations, *Seismol. Res. Lett.* **85,** no. 1, 8–14, doi: 10.1785/0220130083.

Hao, J., C. Ji, W. Wang, and Z. Yao (2013). Rupture history of the 2013 M_w 6.6 Lushan earthquake constrained with local strong motion and teleseismic body and surface waves, *Geophys. Res. Lett.* **40,** no. 20, 5371–5376, doi: 10.1002/2013gl056876.

Hauksson, E., L. M. Jones, and K. Hutton (1995). The 1994 Northridge earthquake sequence in California: Seismological and tectonic aspects, *J. Geophys. Res.* **100,** no. B7, 12,335–12,355, doi: 10.1029/95JB00865.

Jia, K., S. Zhou, J. Zhuang, and C. Jiang (2014). Possibility of the independence between the 2013 Lushan earthquake and the 2008 Wenchuan earthquake on Longmen Shan fault, Sichuan, China, *Seismol. Res. Lett.* **85,** no. 1, 60–67, doi: 10.1785/0220130115.

Jiang, C. S., J. C. Zhuang, F. Long, L. B. Han, and L. J. Guo (2013). Statistical analysis of ETAS parameters in the early stage of the 2013 Lushan M_s 7.0 earthquake sequence, *Acta Seismol. Sinica* **35,** 661–669, doi: 10.3969/j.jssn.0253-3782.2013.05.005 (in Chinese with English abstract).

Lei, J., G. Zhang, and F. Xie (2014). The 20 April 2013 Lushan, Sichuan, mainshock, and its aftershock sequence: Tectonic implications, *Earthq. Sci.* **27,** no. 1, 15–25, doi: 10.1007/s11589-013-0045-9.

Li, Y., D. Jia, M. Wang, J. H. Shaw, J. He, A. Lin, L. Xiong, and G. Rao (2014). Structural geometry of the source region for the 2013 M_w 6.6 Lushan earthquake: Implication for earthquake hazard assessment along the Longmen Shan, *Earth Planet.Sci. Lett.* **390,** 275–286, doi: 10.1016/j.epsl.2014.01.018.

Li, Z., B. Tian, S. Liu, and J. Yang (2013). Asperity of the 2013 Lushan earthquake in the eastern margin of Tibetan plateau from seismic tomography and aftershock relocation, *Geophys. J. Int.* **195,** no. 3, 2016–2022, doi: 10.1093/gji/ggt370.

Liu, C. L., Y. Zheng, C. Ge, X. Xiong, and H. Z. Xu (2013). Rupture process of the M 7.0 Lushan earthquake, 2013, *Sci. China Earth Sci.* **56,** 1187–1192, doi: 10.1007/s11430-013-4639-9.

Liu, J., G. X. Yi, Z. W. Zhang, Z. J. Guan, X. Ruan, F. Long, and F. Du (2013). Introduction to the Lushan, Sichuan M 7.0 earthquake on 20 April 2013, *Chin. J. Geophys.* **56,** 1404–1407, doi: 10.6038/cig20130434 (in Chinese with English abstract).

Liu, M., G. Luo, and H. Wang (2014). The 2013 Lushan earthquake in China tests hazard assessments, *Seismol. Res. Lett.* **85,** no. 1, 40–43, doi: 10.1785/0220130117.

Long, F., X. Z. Wen, X. Ruan, M. Zhao, and G. X. Yi (2015). A more accurate relocation of the 2013 M_s 7. 0 Lushan, Sichuan, China,

earthquake sequence, and the seismogenic structure analysis, *J. Seismol.* 1–13, doi: 10.1007/s10950-015-9485-0.

Lü, J., X. S. Wang, J. R. Su, L. S. Pan, Z. Li, L. W. Yin, X. F. Zeng, and H. Deng (2013). Hypocentral location and source mechanism of M_s 7.0 Lushan earthquake sequence, *Chin. J. Geophys.* **56,** 1753–1763, doi: 10.6038/cjg20130533 (in Chinese with English abstract).

McNamara, D. E., H. M. Benz, R. B. Herrmann, E. A. Bergman, P. Earle, A. Meltzer, M. Withers, and M. Chapman (2013). The M_w 5.8 Mineral, Virginia, earthquake of August 2011 and aftershock sequence: Constraints on earthquake source parameters and fault geometry, *Bull. Seismol. Soc. Am.* **104,** no. 1, 40–54, doi: 10.1785/0120130058.

Miao, M., and S. B. Zhu (2013). The static Coulomb stress change of the 2013 Lushan M_s 7.0 earthquake and its impact on the spatial distribution of aftershocks, *Acta Seismol. Sinica* **35,** 619–631, doi: 10.3969/j.issn.0253-3782.2013.05.001 (in Chinese with English abstract).

Pei, S., H. Zhang, J. Su, and Z. Cui (2014). Ductile gap between the Wenchuan and Lushan earthquakes revealed from the two-dimensional *Pg* seismic tomography, *Scientific Reports* **4,** doi: 10.1038/srep06489.

Peng, Z., and P. Zhao (2009). Migration of early aftershocks following the 2004 Parkfield earthquake, *Nat. Geosci.* **2,** no. 12, 877–881, doi: 10.1038/ngeo697.

Su, J. R., Y. Zheng, J. S. Yang, T. C. Chen, and P. Wu (2013). Accurate locating of the Lushan, Sichuan M 7.0 earthquake on 20 April 2013 and its aftershocks and analysis of the seismogenic structure, *Chin. J. Geophys.* **56,** no. 8, 2636–2644, doi: 10.6038/cjg20130813.

Waldhauser, F., and W. L. Ellsworth (2000). A double-difference earthquake location algorithm: Method and application to the northern Hayward fault, California, *Bull. Seismol. Soc. Am.* **90,** 1353–1368.

Wang, C. Y., W. B. Han, J. P. Wu, H. Lou, and W. W. Chan (2007). Crustal structure beneath the eastern margin of the Tibetan plateau and its tectonic implications, *J. Geophys. Res.* **112,** no. B07307, doi: 10.1029/2005JB003873.

Wang, W. M., J. L. Hao, and Z. X. Yao (2013). Preliminary result for rupture process of Apr. 20, 2013, Lushan earthquake, Sichuan, China, *Chin. J. Geophys.* **56,** 1412–1417, doi: 10.6038/cjg20130436 (in Chinese with English abstract).

Wiemer, S. (2001). A software package to analyze seismicity: ZMAP, *Seismol. Res. Lett.* **72,** 373–382.

Wu, J. P., Y. Huang, T. Z. Zhang, Y. H. Ming, and L. H. Fang (2009). Aftershock distribution of the M_s 8.0 Wenchuan earthquake and three dimensional *P*-wave velocity structure in and around source region, *Chin. J. Geophys.* **52,** 320–328 (in Chinese with English abstract).

Wyss, M. (1973). Towards a physical understanding of the earthquake frequency distribution, *Geophys. J. Roy. Astron. Soc.* **31,** 341–359.

Xu, C., and X. Xu (2014). The spatial distribution pattern of landslides triggered by the 20 April 2013 Lushan earthquake of China and its implication to identification of the seismogenic fault, *Chin. Sci. Bull.* **59,** no. 13, 1416–1424, doi: 10.1007/s11434-014-0202-0.

Xu, X. W., X. Z. Wen, Z. J. Han, G. H. Chen, C. Y. Li, W. J. Zheng, S. M. Zhang, Z. K. Ren, C. Xu, X. B. Tan, *et al.* (2013). Lushan M_s 7.0 earthquake: A blind reserve-fault earthquake, *Chin. Sci. Bull.* **58,** 3437–3443, doi: 10.1007/s11434-013-5999-4.

Yi, G. X., X. Z. Wen, H. Xin, H. Z. Qiao, S. W. Wang, and Y. Gong (2013). Stress state and major-earthquake risk on the southern segment of the Longmenshan fault zone, *Chin. J. Geophys.* **56,** no. 4, 9, doi: 10.6038/cjg20130407.

Zeng, X. F., Y. Luo, L. B. Han, and Y. L. Shi (2013). The Lushan M_s 7.0 earthquake on 20 April, 2013: A high-angle thrust event, *Chin. J. Geophys.* **56,** no. 4, 1418–1424, doi: 10.6038/cjg20130407 (in Chinese with English abstract).

Zhang, G. W., and J. S. Lei (2013). Relocations of Lushan, Sichuan strong earthquake (M_s) 7.0 and its aftershocks, *Chin. J. Geophys.* **56,** 1764–1771, doi: 10.6038/cjg20130534 (in Chinese with English abstract).

Zhang, Y. Q., S. W. Dong, C. T. Hou, J. S. Shi, Z. H. Wu, H. L. Li, P. Sun, G. Liu, and J. Li (2013). Seismogenic structure of the April 20, 2013, Lushan M_s 7 earthquake in Sichuan, *Acta Geol. Sinica* (English edition) **87,** no. 3, 633–645.

Zhang, Y., L. S. Xu, and Y. T. Chen (2013). Rupture of the Lushan 4.20 earthquake and preliminary analysis on the disaster-causing mechanism, *Chin. J. Geophys.* **56,** 1408–1411, doi: 10.6038/cjg20130435 (in Chinese with English abstract).

Zhao, B., Y. Gao, Z. B. Huang, X. Jiang, and D. H. Li (2013). Double-difference relocation, focal mechanism and stress inversion of Lushan M_s 7.0 earthquake sequence, *Chin. J. Geophys.* **56,** 3385–3395, doi: 10.6038/cjg20131014 (in Chinese with English abstract).

Zhao, C. P., L. Q. Zhou, and Z. L. Chen (2013). Source rupture process of Lushan M_s 7.0 earthquake, Sichuan, China and its tectonic implication, *Chin. Sci. Bull.* **58,** 3444–3450, doi: 10.1007/s11434-013-6017-6.

Zhao, D., A. Hasegawa, and S. Horiuchi (1992). Tomographic imaging of *P* and *S* wave velocity structure beneath northeastern Japan, *J. Geophys. Res.* **97,** 19,909–19,928, doi: 10.1029/92JB00603.

Zhao, D., A. Hasegawa, and H. Kanamori (1994). Deep structure of Japan subduction zone as derived from local, regional, and teleseismic events, *J. Geophys. Res.* **99,** 22,313–22,329, doi: 10.1029/94JB01149.

Lihua Fang
Jianping Wu
Weilai Wang
Changzai Wang
Ting Yang
Yan Cai
Institute of Geophysics
China Earthquake Administration
Beijing 100081, China
flh@cea-igp.ac.cn

Wenkang Du
Jinrong Su
Earthquake Administration of Sichuan Province
No. 29, South Renmin Road, section 3
Chengdu 610041 Sichuan, China

Published Online 3 June 2015